

PAPER

Joint Tomlinson-Harashima Precoding and Frequency-Domain Equalization for Broadband Single-Carrier Transmission

Kazuki TAKEDA^{†a)}, Hiromichi TOMEBA[†], *Student Members*, and Fumiyuki ADACHI[†], *Fellow*

SUMMARY The performance of single-carrier (SC) transmission in a frequency-selective fading channel degrades due to a severe inter-symbol interference (ISI). Using frequency-domain equalization (FDE) based on the minimum mean square error (MMSE) criterion can improve the bit error rate (BER) performance of SC transmission. However, the residual ISI after FDE limits the performance improvement. In this paper, we propose a joint use of Tomlinson-Harashima precoding (THP) and FDE to remove the residual ISI. An approximate conditional BER analysis is presented for the given channel condition. The achievable average BER performance is evaluated by Monte-Carlo numerical computation method using the derived conditional BER. The BER analysis is confirmed by computer simulation of the signal transmission.

key words: single-carrier, frequency-domain equalization, Tomlinson-Harashima precoding

1. Introduction

In the next generation mobile communication systems, high speed and high quality data services are demanded [1]. If single-carrier (SC) transmission is used, its transmission performance significantly degrades due to inter-symbol interference (ISI) arising from severe frequency-selective fading channel [2]. It was shown that frequency-domain equalization (FDE) based on the minimum mean square error (MMSE) criterion can improve the bit error rate (BER) performance of SC transmission [3], [4]. However, due to the residual ISI after FDE, the BER performance is still far from the theoretical lower bound. Therefore, ISI cancellation techniques have been intensively studied [5]–[7]. Another way to remove the residual ISI is the application of Tomlinson-Harashima precoding (THP) [8], [9], which recently has been attracting attention [10]–[12]. In this paper, we propose a joint use of THP and FDE for SC transmission in a frequency-selective fading channel. The channel seen after FDE is called the equivalent channel. We try to use THP in order to remove the residual ISI after FDE. However, since the equivalent channel is characterized by a non-causal filter, THP cannot be directly applied. We apply QR-decomposition to transform the non-causal equivalent channel into a causal channel. With the perfect knowledge of the channel state information (CSI) at both the transmitter and the receiver, ISI can be perfectly removed by joint THP/FDE.

The reminder of this paper is organized as follows. Joint THP/FDE is described in Sect. 2. An approximate conditional BER analysis is presented for the given channel condition in Sect. 3. In Sect. 4, the achievable average BER performance in a frequency-selective fading channel is evaluated by Monte-Carlo numerical computation method using the derived conditional BER. The BER analysis is confirmed by computer simulation. This paper is concluded in Sect. 5.

2. Joint THP/FDE

The overall system model of SC transmission using joint THP/FDE is illustrated in Fig. 1. In this paper, CSI is assumed to be perfectly known at both the transmitter and the receiver. Furthermore, throughout this paper, the symbol-spaced discrete-time signal representation is used. The propagation channel is assumed to be an L -path frequency-selective fading channel. The channel impulse response is given by

$$h(\tau) = \sum_{l=0}^{L-1} h_l \delta(\tau - \tau_l), \quad (1)$$

where h_l and τ_l are respectively the complex valued path gain with $E \left[\sum_{l=0}^{L-1} |h_l|^2 \right] = 1$ and the time delay of the l th path. We assume a symbol-spaced time delay; the l th path time delay is l symbols, i.e., $\tau_l = l$.

Before introducing THP, we discuss the case of FDE

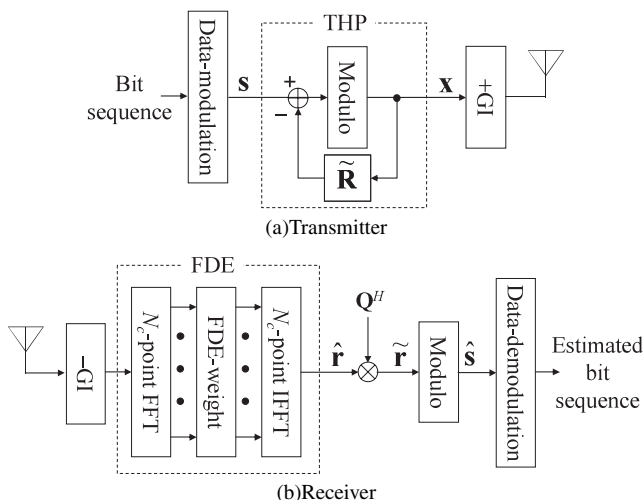


Fig. 1 Transmission system model of joint THP/FDE.

Manuscript received November 22, 2006.

Manuscript revised June 5, 2007.

[†]The authors are with the Department of Electrical and Communication Engineering, Graduate School of Engineering, Tohoku University, Sendai-shi, 980-8579 Japan.

a) E-mail: kazuki@mobile.ecei.tohoku.ac.jp

DOI: 10.1093/ietcom/e91-b.1.258

only. We consider three FDE weights based on equal gain (EQ) criterion, maximal ratio (MR) criterion, and the MMSE criterion. Then, we introduce the equivalent channel gain to discuss the residual ISI after FDE.

2.1 FDE and Residual ISI

At the transmitter, the data-modulated symbol sequence is divided into a sequence of data symbol block of N_c symbols each, where N_c is the size of fast Fourier transform (FFT). Each symbol block is transmitted after inserting the cyclic prefix into the guard interval (GI). The transmitted symbol block is received via a frequency-selective fading channel. The GI-removed received signal block can be expressed using the vector form as

$$\mathbf{r} = [r(0), \dots, r(N_c - 1)]^T = \sqrt{\frac{2E_s}{T_s}} \mathbf{h} \mathbf{s} + \mathbf{n}, \quad (2)$$

where E_s and T_s are respectively the average transmit energy per symbol and the symbol duration, $\mathbf{s} = [s(0), \dots, s(N_c - 1)]^T$ is the data symbol block, \mathbf{h} is the $N_c \times N_c$ channel matrix, and $\mathbf{n} = [n(0), \dots, n(N_c - 1)]^T$ is the noise vector. \mathbf{h} is given as

$$\mathbf{h} = \begin{bmatrix} h_0 & 0 & \cdots & 0 & h_{L-1} & \cdots & h_1 \\ \vdots & h_0 & \ddots & & \ddots & \ddots & \vdots \\ \vdots & \vdots & \ddots & \ddots & & \ddots & h_{L-1} \\ h_{L-1} & \vdots & & h_0 & \ddots & & 0 \\ 0 & h_{L-1} & & \vdots & h_0 & \ddots & \vdots \\ \vdots & \ddots & \ddots & \vdots & & \ddots & 0 \\ 0 & \cdots & 0 & h_{L-1} & \cdots & \cdots & h_0 \end{bmatrix}, \quad (3)$$

$$\mathbf{h}_{i,j} = \begin{cases} h_{(j-i) \bmod N_c}, & |j-i| < L \\ 0, & |j-i| \geq L \end{cases}$$

and $n(t)$ is a zero-mean additive white Gaussian noise (AWGN) having a variance of $2N_0/T_s$ (N_0 is the one-sided power spectrum density).

N_c -point FFT is applied to transform the received signal block into a frequency-domain signal $\{R(k); k = 0 \sim N_c - 1\}$. The k th frequency component $R(k)$ is multiplied by the FDE weight $w(k)$. Then, N_c -point inverse FFT (IFFT) is applied to transform the frequency-domain signal $\{R(k)w(k)\}$ back to the time-domain signal block $\hat{\mathbf{r}}$. $\hat{\mathbf{r}}$ can be expressed as

$$\hat{\mathbf{r}} = [\hat{r}(0), \dots, \hat{r}(N_c - 1)]^T = \sqrt{\frac{2E_s}{T_s}} \hat{\mathbf{h}} \mathbf{s} + \hat{\mathbf{n}}, \quad (4)$$

where $\hat{\mathbf{h}}$ is the $N_c \times N_c$ equivalent channel matrix after FDE and $\hat{\mathbf{n}} = [\hat{n}(0), \dots, \hat{n}(N_c - 1)]^T$ is the noise vector after FDE. $\hat{\mathbf{h}}$ is given as

$$\hat{\mathbf{h}} = \begin{bmatrix} \hat{h}_0 & \hat{h}_{-1} & \hat{h}_{-2} & \cdots & \cdots & \hat{h}_2 & \hat{h}_1 \\ \hat{h}_1 & \hat{h}_0 & \hat{h}_{-1} & \hat{h}_{-2} & & & \hat{h}_2 \\ \vdots & \ddots & \ddots & \ddots & \ddots & & \vdots \\ \vdots & \hat{h}_2 & \hat{h}_1 & \hat{h}_0 & \hat{h}_{-1} & \hat{h}_{-2} & \vdots \\ \vdots & & \hat{h}_2 & \hat{h}_1 & \hat{h}_0 & \hat{h}_{-1} & \hat{h}_{-2} \\ \vdots & & & \ddots & \ddots & \ddots & \vdots \\ \hat{h}_{-1} & \hat{h}_{-2} & \cdots & \cdots & \hat{h}_2 & \hat{h}_1 & \hat{h}_0 \end{bmatrix} \quad (5)$$

$$\hat{\mathbf{h}}_{i,j} = \hat{h}_{(j-i) \bmod N_c}$$

with

$$\hat{h}_l = \frac{1}{N_c} \sum_{k=0}^{N_c-1} H(k) w(k) \exp\left(j2\pi k \frac{l}{N_c}\right), \quad (6)$$

where $H(k)$ and $w(k)$ are respectively the channel gain and FDE weight at the k th frequency given by [13]

$$H(k) = \sum_{l=0}^{L-1} h_l \exp\left(-j2\pi k \frac{l}{N_c}\right) \quad (7)$$

$$w(k) = \begin{cases} \frac{H^*(k)}{|H(k)|}, & \text{EGC} \\ H^*(k), & \text{MRC} \\ \frac{H^*(k)}{|H(k)|^2 + (E_s/N_0)^{-1}}, & \text{MMSE.} \end{cases} \quad (8)$$

The equivalent channel matrix is not a diagonal matrix and therefore the residual ISI is produced. The use of MMSE-FDE significantly improves the BER performance. However, the residual ISI limits the performance improvement and the achievable BER performance with MMSE-FDE is still far from the theoretical lower bound [5].

2.2 Joint THP/FDE

To suppress the residual ISI, we use THP at the transmitter. However, since the impulse response of the equivalent channel is a circular convolution between those of the channel and FDE filter, it is spread not only over $\tau > 0$ but also over $\tau < 0$ and therefore, the equivalent channel can be viewed as a non-causal channel. This implies that direct application of THP cannot remove completely the residual ISI after FDE. We apply QR-decomposition [14] on $\hat{\mathbf{h}}$ to transform the non-causal channel into a causal channel. Using a unitary matrix \mathbf{Q} and an upper triangular matrix \mathbf{R} , $\hat{\mathbf{h}}$ can be expressed as

$$\hat{\mathbf{h}} = \mathbf{Q} \mathbf{R}$$

$$= \begin{bmatrix} Q_{0,0} & \cdots & Q_{0,N_c-1} \\ \vdots & \ddots & \vdots \\ Q_{N_c-1,0} & \cdots & Q_{N_c-1,N_c-1} \end{bmatrix} \begin{bmatrix} R_{0,0} & \cdots & R_{0,N_c-1} \\ & \ddots & \vdots \\ \mathbf{0} & & R_{N_c-1,N_c-1} \end{bmatrix}. \quad (9)$$

At the transmitter, THP transforms an N_c -symbol block $\mathbf{s} = [s(0), \dots, s(N_c - 1)]^T$ into a pre-equalized signal block $\mathbf{x} = [x(0), \dots, x(N_c - 1)]^T$. \mathbf{x} is expressed as

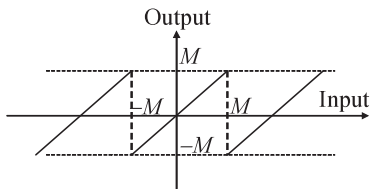


Fig. 2 Input-output property of the modulo operator.

$$\mathbf{x} = \mathbf{s} - \tilde{\mathbf{R}}\mathbf{x} + 2M\mathbf{z}_t, \quad (10)$$

where $\tilde{\mathbf{R}}$ is the feedback coefficient matrix of THP, which is obtained from the QR-decomposition of $\hat{\mathbf{h}}$, and the (i, j) th component of $\tilde{\mathbf{R}}$ is given by

$$\tilde{R}_{i,j} = \begin{cases} R_{i,j}/R_{i,i}, & i < j \\ 0, & i \geq j \end{cases}. \quad (11)$$

In Eq. (10), $2M\mathbf{z}_t = [2Mz_t(0), \dots, 2Mz_t(N_c - 1)]^T$ represents the modulo- $2M$ operation [15]. To prevent the transmit signal amplitude increase, THP uses the modulo operator. The real and imaginary parts of $z_t(t)$ are integers, which are implicitly decided symbol-by-symbol by the modulo operator to reduce the real and imaginary parts of $x(t)$ into the interval $[-M, M)$, where the modulo operation size M depends on the data modulation scheme; $M = \sqrt{2}$ for QPSK, $M = 4/\sqrt{10}$ for 16 QAM, $M = 8/\sqrt{42}$ for 64 QAM. The input-output property of the modulo operator is illustrated in Fig. 2.

After the insertion of an N_g -sample GI, the pre-equalized signal block \mathbf{x} is transmitted. At the receiver, the GI-removed received signal block is transformed by N_c -point FFT into the frequency-domain signal. Then, FDE is performed and IFFT is applied to the frequency-domain signal to obtain the time-domain signal block $\hat{\mathbf{r}}$, which can be expressed as

$$\hat{\mathbf{r}} = \sqrt{\frac{2E_s}{T_s}} \hat{\mathbf{h}}\mathbf{x} + \hat{\mathbf{n}}. \quad (12)$$

Then, $\hat{\mathbf{r}}$ is multiplied by \mathbf{Q}^H to obtain $\tilde{\mathbf{r}}$, where $(\cdot)^H$ represents the Hermitian transposition. Using Eqs. (10) and (12), we have

$$\begin{aligned} \tilde{\mathbf{r}} &= \mathbf{Q}^H \hat{\mathbf{r}} = \sqrt{\frac{2E_s}{T_s}} \mathbf{R}\mathbf{x} + \mathbf{Q}^H \hat{\mathbf{n}} \\ &= \sqrt{\frac{2E_s}{T_s}} \begin{bmatrix} R_{0,0} & \mathbf{0} \\ & \ddots \\ \mathbf{0} & R_{N_c-1, N_c-1} \end{bmatrix} (\mathbf{s} + 2M\mathbf{z}_t) + \mathbf{Q}^H \hat{\mathbf{n}}. \end{aligned} \quad (13)$$

To recover the transmit symbol block \mathbf{s} , the signal transposition by using the transmitter modulo operation (i.e., $2M\mathbf{z}_t$ in Eq. (10)) needs to be removed from Eq. (13). This can be easily done by dividing $\tilde{\mathbf{r}}$ by $\sqrt{2E_s/T_s} \text{diag}(\mathbf{R})$, where \mathbf{R} is an upper triangular matrix as shown in Eq. (9), and inputting the result to the same modulo operator as used in the transmitter. The modulo operator output $\hat{\mathbf{s}}$ is given as

$$\begin{aligned} \hat{\mathbf{s}} &= \left(\frac{2E_s}{T_s}\right)^{-\frac{1}{2}} \begin{bmatrix} R_{0,0}^{-1} & & \mathbf{0} \\ & \ddots & \\ \mathbf{0} & & R_{N_c-1, N_c-1}^{-1} \end{bmatrix} \tilde{\mathbf{r}} + 2M\mathbf{z}_r \\ &= \mathbf{s} + 2M(\mathbf{z}_t + \mathbf{z}_r) + \left(\frac{2E_s}{T_s}\right)^{-\frac{1}{2}} \begin{bmatrix} R_{0,0}^{-1} & & \mathbf{0} \\ & \ddots & \\ \mathbf{0} & & R_{N_c-1, N_c-1}^{-1} \end{bmatrix} \mathbf{Q}^H \hat{\mathbf{n}}, \end{aligned} \quad (14)$$

which is the decision variable associated with the data symbol block \mathbf{s} . In Eq. (14), $2M\mathbf{z}_r = [2Mz_r(0), \dots, 2Mz_r(N_c - 1)]^T$ represents the modulo- $2M$ operation and the first and third terms are respectively the desired signal and noise. If the noise is negligible, \mathbf{z}_r is equal to $-\mathbf{z}_t$ always. Therefore, the transmitted data symbol block \mathbf{s} is correctly recovered at the receiver. However, the modulo operation error due to the noise happens actually, thereby producing the decision error.

3. BER Analysis

We consider QPSK, 16 QAM, and 64 QAM for data modulation. The noise distorts the modulo operation at the receiver and sometimes the received signal is shifted to a wrong position. Assuming a high SNR, the distortion of the modulo operation rarely happens and the modulo operation error (i.e., $\mathbf{z}_r \neq -\mathbf{z}_t$) due to the noise can be neglected for the analysis. Therefore, we assume $\mathbf{z}_r = -\mathbf{z}_t$ in Eq. (13) and we have

$$\tilde{\mathbf{r}} = \sqrt{\frac{2E_s}{T_s}} \begin{bmatrix} R_{0,0} & & \mathbf{0} \\ & \ddots & \\ \mathbf{0} & & R_{N_c-1, N_c-1} \end{bmatrix} \mathbf{s} + \mathbf{Q}^H \hat{\mathbf{n}}. \quad (15)$$

The i th element $\tilde{r}(i)$ of $\tilde{\mathbf{r}}$ is given by

$$\tilde{r}(i) = \sqrt{\frac{2E_s}{T_s}} R_{i,i} s(i) + \psi(i), \quad (16)$$

where $\psi(i)$ is the i th element of $\mathbf{Q}^H \hat{\mathbf{n}}$ and is a zero-mean complex Gaussian noise. The noise power is given by (see Appendix A)

$$\sigma^2(i) = \frac{1}{2} E[|\psi(i)|^2] = \frac{1}{N_c} \frac{N_0}{T_s} \sum_{k=0}^{N_c-1} |w(k)|^2 |Q_i(k)|^2, \quad (17)$$

where

$$Q_i(k) = \sum_{p=0}^{N_c-1} Q_{i,p} \exp\left(-j2\pi k \frac{p}{N_c}\right). \quad (18)$$

The approximate conditional BER (it is an exact expression for QPSK) of the i th symbol in the transmitted signal block \mathbf{s} for the given \mathbf{h} is given as [16]

$$p_b^{(i)}\left\{\frac{E_s}{N_0}, \mathbf{h}\right\} = \begin{cases} \frac{1}{2} \operatorname{erfc}\left[\sqrt{\frac{1}{4}\gamma^{(i)}\left(\frac{E_s}{N_0}, \mathbf{h}\right)}\right], & \text{QPSK} \\ \frac{3}{8} \operatorname{erfc}\left[\sqrt{\frac{1}{20}\gamma^{(i)}\left(\frac{E_s}{N_0}, \mathbf{h}\right)}\right], & \text{16QAM} \\ \frac{7}{24} \operatorname{erfc}\left[\sqrt{\frac{1}{84}\gamma^{(i)}\left(\frac{E_s}{N_0}, \mathbf{h}\right)}\right], & \text{64QAM,} \end{cases} \quad (19)$$

where $\operatorname{erfc}[x] = 2/\sqrt{\pi} \int_x^\infty \exp(-t^2) dt$ is the complementary error function and $\gamma^{(i)}(E_s/N_0, \mathbf{h})$ is the conditional SNR, given as

$$\gamma^{(i)}\left(\frac{E_s}{N_0}, \mathbf{h}\right) = \frac{E_s}{N_0} \frac{2|R_{i,i}|^2}{\sigma^2(i)}. \quad (20)$$

The approximate average BER can be numerically evaluated by averaging Eq. (19) over all possible realizations of \mathbf{h} .

It can be seen from Eq. (16) that the channel can be transformed into the frequency non-selective channel and its channel gain is given by $R_{i,i}$. The received SNR is in proportion to $|R_{i,i}|^2$. Figure 3 plots the distribution of $|R_{i,i}|^2$ in a block of $N_c=128$ symbols. The value of $|R_{i,i}|^2$ drops at symbol positions close to the end of the block. The reason for this is discussed in Appendix B.

This indicates that the BER of the symbol near the end of the block is worse compared to those of other symbols. To avoid the BER degradation, we insert $N_d (=N_g)$ dummy symbols in the block as shown in Fig. 4. Although this dummy symbol insertion reduces the transmission efficiency to $(N_c - N_d)/(N_c + N_g)$, the block-averaged BER can

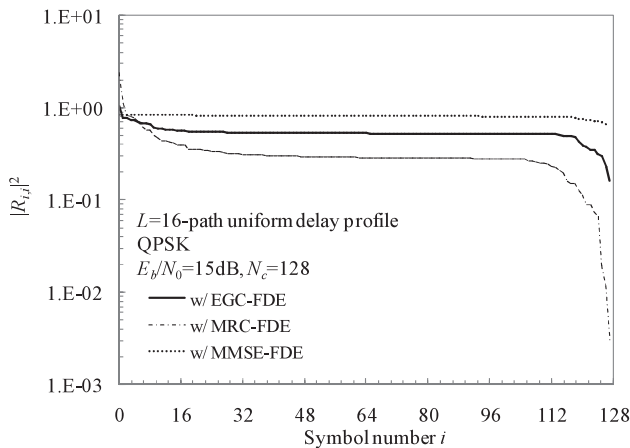


Fig. 3 $|R_{i,i}|^2$.

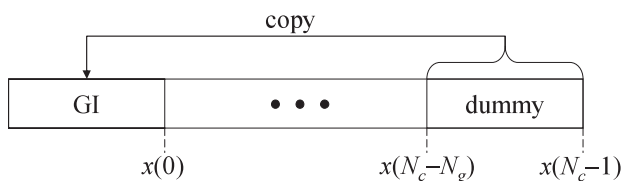


Fig. 4 Block structure.

be improved.

4. Numerical and Simulation Results

The simulation condition is summarized in Table 1. The channel is assumed to be a symbol-spaced $L=16$ -path frequency-selective block Rayleigh fading channel. Ideal channel estimation is assumed.

The achievable average BER is evaluated by Monte-Carlo numerical computation method. First, we generate a set of path gains $\{h_l; l = 0 \sim L - 1\}$ for obtaining the FDE weight $\{w(k); k = 0 \sim N_c - 1\}$ using Eq. (8) and the equivalent channel matrix $\hat{\mathbf{h}}$ using Eqs. (5) and (6). After performing QR-decomposition on $\hat{\mathbf{h}}$ to obtain the matrices \mathbf{Q} and \mathbf{R} , the conditional BER of the i th symbol in the block for the given average transmit E_s/N_0 is computed using Eq. (19). This BER computation is repeated a sufficient number of times to obtain the theoretical average BER $P_b(i)$ of the i th symbol. Then, the block averaged BER is obtained by averaging

Table 1 Simulation condition.

Transmitter	Data-modulation	QPSK, 16QAM, 64QAM
	Block length	$N_c=128$
	GI length	$N_g=16$
	No. of dummy symbols	$N_d=16(=N_g)$
	Modulo operation size	$M = \begin{cases} \sqrt{2}, & \text{QPSK} \\ 4/\sqrt{10}, & \text{16QAM} \\ 8/\sqrt{42}, & \text{64QAM} \end{cases}$
Channel model	Fading type	Frequency-selective block Rayleigh fading
	No. of paths	$L=16$
	Power delay profile	Uniform
	Time delay	$\tau=l(l=0 \sim L-1)$
Receiver	FDE	EGC, MRC, MMSE

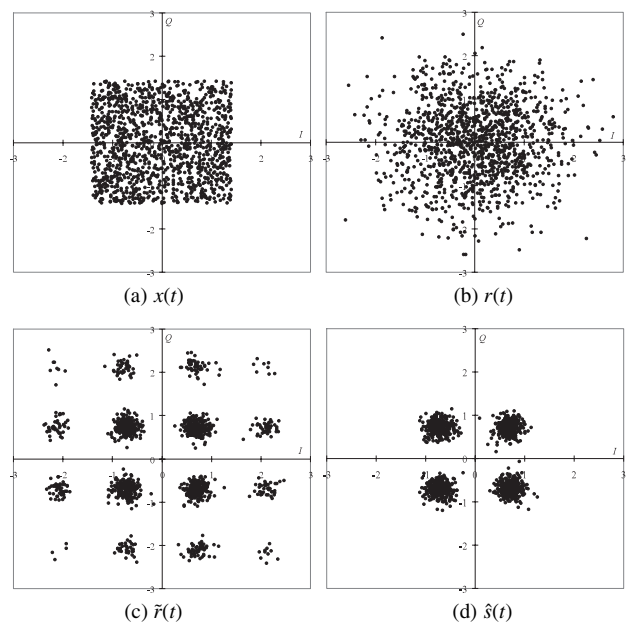


Fig. 5 Signal distribution.

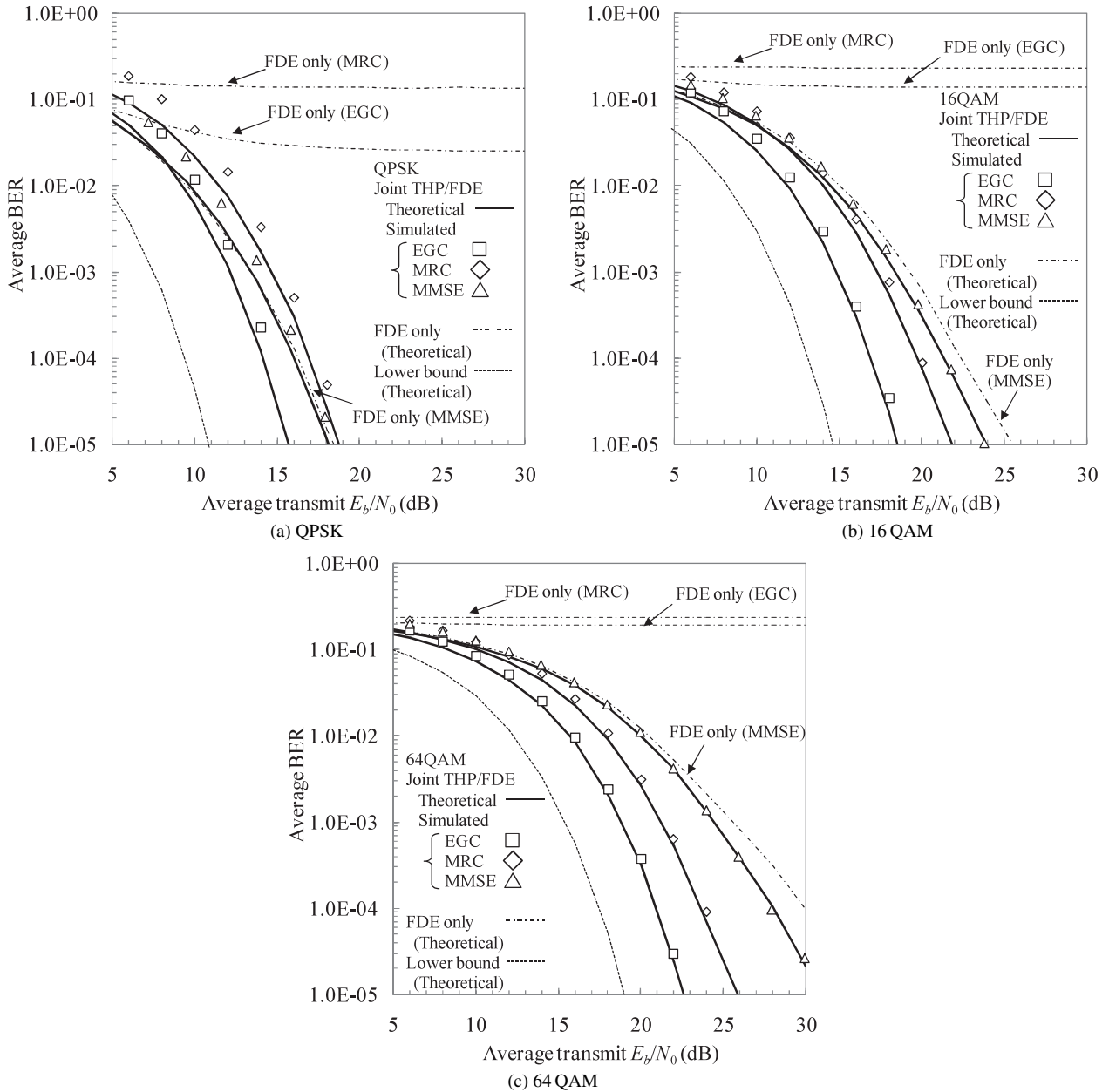


Fig. 6 BER performance comparison.

$P_b(i)$ for $i = 0 \sim N_c - N_d - 1$. The computer simulation is also carried out to obtain the average BER to confirm the validity of the BER analysis.

The signal distribution in (I, Q) -plane is shown in Fig. 5 for the case of QPSK data modulation and joint THP/EGC-FDE at the average transmit bit energy-to-noise power spectrum density $E_b/N_0 (=0.5(E_s/N_0)(N_c + N_g)/(N_c - N_d))=15$ dB. From Fig. 5(a), it can be seen that THP output $x(t)$ is distributed randomly in an entire region, $-M \leq \text{Re}[x(t)]$ and $\text{Im}[x(t)] < M$. The distribution of the received signal $r(t)$ is shown in Fig. 5(b). Since $\tilde{r}(t)$ has the $2Mz_t(t)$ term, the distribution of $\tilde{r}(t)$ looks like 16 QAM as shown in Fig. 5(c). To obtain the proper signal distribution, the $2Mz_t(t)$ term must be removed from $\tilde{r}(t)$. This is done by

modulo operation. The modulo operator output $\hat{s}(t)$ gives the QPSK signal distribution as shown in Fig. 5(d).

The theoretical and computer-simulated average BER performances are plotted in Fig. 6 as a function of the average transmit $E_b/N_0 (=1/N(E_s/N_0)(N_c + N_g)/(N_c - N_d))$ for QPSK ($N=2$), 16 QAM ($N=4$), 64 QAM ($N=6$). In Fig. 6, the theoretical BER performance using FDE only is plotted for EGC, MRC, and MMSE. Using EGC or MRC-FDE only, BER floor is produced by the residual ISI [13]. However, by using joint THP/FDE, the residual ISI is suppressed and the BER performance is significantly improved. It is seen from Fig. 6 that joint THP/EGC-FDE provides the best BER performance. Below, we discuss why this happens. The BER performance of joint THP/FDE depends on the

SNR given by Eq. (20). There may be two factors which affect the SNR. The first one is the SNR achievable by using FDE only. The second is the signal power loss after QR-decomposition.

First, we discuss the SNR achievable by using FDE only. The SNR when using FDE only depends on the frequency diversity gain of FDE. Using FDE only, MRC can maximize the frequency diversity gain since it is matched to the channel and accordingly achieves the largest SNR. In the case of EGC, the magnitude of equalization weight is the same for all frequencies and therefore, the frequency diversity gain is smaller than MRC. On the other hand, since MMSE suppresses the channel frequency-selectivity seen after FDE in order to minimize the sum of spectrum distortion and the noise, the frequency diversity gain is lower than that of EGC (it should be noted that since the spectrum distortion is lowered, the residual ISI after FDE can be minimized and therefore MMSE-FDE provides the best BER performance when using FDE only [17]). As a consequence, the achievable SNR using FDE only is the largest with MRC and is the smallest with MMSE.

Next, we discuss the power loss due to QR-decomposition. The signal power after multiplying \mathbf{Q}^H is in proportion to the squared value of the diagonal component of \mathbf{R} (see Eq. (20)), which is affected by the correlation between the two column vectors of $\hat{\mathbf{h}}$. The correlation is stronger for MRC than for EGC and hence, the signal power loss is larger for MRC. On the other hand, since $\hat{\mathbf{h}}$ of MMSE is close to an orthogonal matrix, the signal power loss is minimal (see Appendix B). The above intuitive discussion can be summarized as follows. MRC can maximize the SNR when using FDE only, but produces the largest power loss when jointly using THP and FDE. MMSE can minimize the power loss when jointly using THP and FDE, but achieves the lowest SNR when using FDE only. On the other hand, EGC can achieve the SNR close to MRC when using FDE only and furthermore, the power loss is not that much when jointly using THP and FDE. Therefore, it can be concluded that EGC provides the best BER performance. A detailed and theoretical analysis is left as an important future study.

When QPSK data modulation is used, joint THP/FDE slightly improves the BER performance compared to that of MMSE-FDE only. As the modulation level increases, decision error is produced more likely due to the residual ISI and therefore, the BER performance using MMSE-FDE only significantly degrades. However, joint THP/FDE significantly improves the BER performance compared to the use of MMSE-FDE only since the residual ISI can be perfectly cancelled (we are assuming perfect channel estimation).

The modulo operation error, i.e., $z_r \neq z_t$, is sometimes produced due to the noise. The modulo operation error is most likely produced for the symbols closest to the modulo operation boundary. For 64 QAM, only 28 symbols out of a total of 64 symbols have the closest distance to the modulo operation boundary, but all four symbols are facing the boundary for QPSK. In the theoretical analysis, the modulo

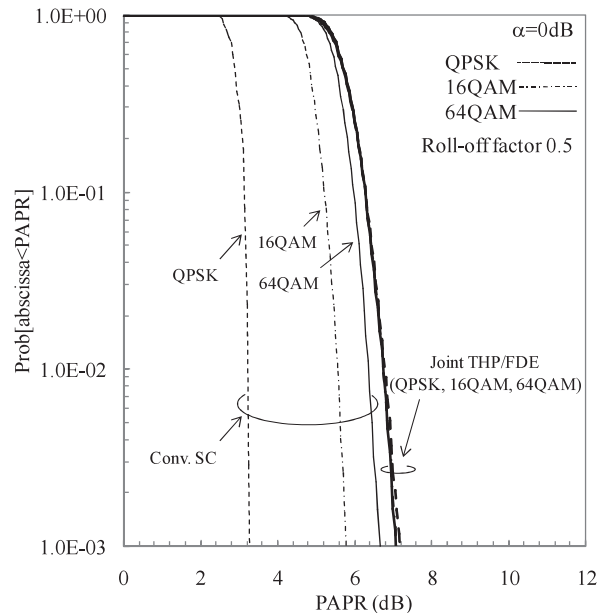


Fig. 7 PAPR distribution.

operation error is ignored. Therefore, the theoretical BER is lower than an exact one, but gets closer as the modulation level gets higher. However, over all, a good agreement between the theoretical and simulated BER performance can be seen. This confirms the validity of our analysis.

THP increases the peak-to-average power ratio (PAPR) of the transmit signal. However, the modulo operator used in THP can suppress the PAPR. Figure 7 plots the probability of the PAPR exceeding the abscissa, $\text{Prob}[\text{abscissa} < \text{PAPR}]$, when joint THP/FDE is used. A root raised cosine Nyquist filter with a roll-off factor of 0.5 [16], [18] is assumed for SC using THP/FDE. For the conventional SC transmission, PAPR increases as the modulation level increases. Although the use of THP with modulo operation increases the PAPR, the output signal has almost the same PAPR distribution irrespective of the modulation level.

The PAPR distribution of joint THP/FDE depends on the degree of channel frequency-selectivity. Figure 8 shows the PAPR distribution of joint THP/EGC-FDE with the path decay factor α as a parameter. QPSK data-modulation is assumed. For comparison, the PAPR distribution of orthogonal frequency division multiplexing (OFDM) is also plotted in Fig. 8. When $\alpha = \infty$ dB (equivalent to the frequency non-selective single path case), the PAPR distribution of joint THP/FDE coincides with that of conventional SC transmission. As α decreases (or the frequency-selectivity get stronger), the PAPR of joint THP/FDE tends to increase; however, it is still much lower than that of OFDM since the modulo operator used in THP limits the peak transmit power. It can be seen from Fig. 8 that if $\alpha < 12$ dB, joint THP/FDE lowers the PAPR level at $\text{CCDF}=0.01$ by about 3 dB compared to OFDM.

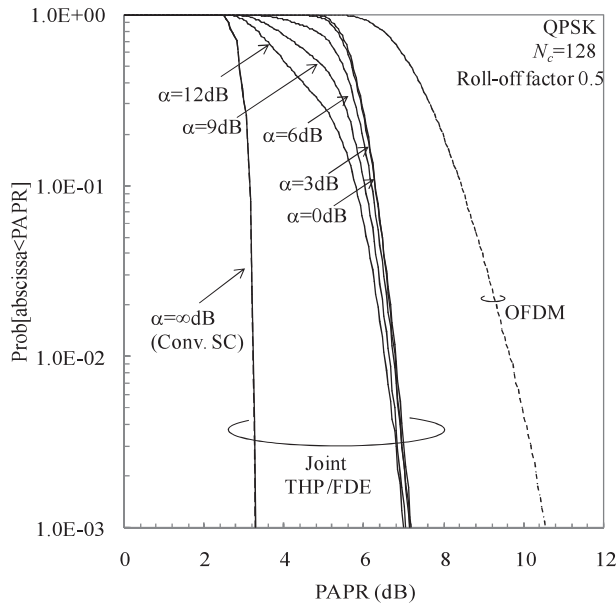


Fig. 8 Impact of channel selectivity on PAPR distribution.

5. Conclusions

In this paper, we proposed joint THP/FDE for SC transmission in a frequency-selective fading channel. THP is used at the transmitter in order to remove the residual ISI after FDE. We derived the approximate conditional BER for the given channel condition and evaluated the achievable average BER by Monte-Carlo numerical computation method. The BER analysis was confirmed by computer simulation. We have shown that the BER performance is significantly improved by using joint THP/FDE compared to that of MMSE-FDE only. The performance improvement was found to be more significant for higher level modulation.

In this paper, we considered MRC, EGC, and MMSE equalization weights and found that EGC weight gives the best BER performance when joint THP/FDE is used. However, the EGC weight may not be optimal. Finding the optimal equalization weight is another interesting future study topic. We assumed ideal channel estimation. Joint THP/FDE requires the knowledge of CSI at both the transmitter and the receiver. Imperfect channel estimation reduces the BER performance improvement predicted by the analysis. We also assumed an ideal linear transmit power amplifier. Since the introduction of THP increases the PAPR as shown in Figs. 7 and 8, it is important to investigate how the non-linearity of the transmit power amplifier degrades the BER performance. Impacts of the channel estimation error and the power amplifier nonlinearity are left as important future study topics.

References

- [1] F. Adachi, "Wireless past and future-evolving mobile communications systems," IEICE Trans. Fundamentals, vol.E84-A, no.1, pp.55-60, Jan. 2001.
- [2] W.C. Jakes Jr., ed., Microwave Mobile Communications, Wiley, New York, 1974.
- [3] D. Falconer, S.L. Ariyavitakul, A. Benyamin-Seeyar, and B. Eidson, "Frequency domain equalization for single-carrier broadband wireless systems," IEEE Commun. Mag., vol.40, no.4, pp.58-66, April 2002.
- [4] F. Adachi, D. Garg, S. Takaoka, and K. Takeda, "Broadband CDMA techniques," IEEE Wirel. Commun. Mag., vol.12, no.2, pp.8-18, April 2005.
- [5] K. Takeda and F. Adachi, "Iterative frequency-domain inter-chip interference cancellation for DS-SS-CDMA," Proc. IEEE 8th Wireless Personal Multimedia Communications (WPMC), pp.759-763, Aalborg, Denmark, Sept. 2005.
- [6] K. Ishihara, K. Takeda, and F. Adachi, "Frequency-domain multi-stage MAI cancellation for DS-SS-CDMA uplink with transmit/receive antenna diversity," Proc. IEEE 62nd Vehicular Technology Conference (VTC), vol.1, pp.78-82, Dallas, TX, Sept. 2005.
- [7] Y. Zhu and K.B. Letaief, "Single-carrier frequency-domain equalization with decision-feedback processing for time-reversal space-time block coded systems," IEEE Trans. Commun., vol.53, no.7, pp.1127-1131, July 2005.
- [8] M. Tomlinson, "New automatic equalizer employing modulo arithmetic," Electron. Lett., vol.7, no.5/6, pp.138-139, March 1971.
- [9] H. Harashima and H. Miyakawa, "Matched-transmission technique for channels with intersymbol interference," IEEE Trans. Commun., vol.20, no.4, pp.774-780, Aug. 1972.
- [10] R. Fischer, C. Windpassinger, A. Lampe, and J. Huber, "Space-time transmission using Tomlinson-Harashima precoding," Proc. 4th Intern. ITG Conference on Source and Channel Coding, pp.139-147, Berlin, Jan. 2002.
- [11] C. Windpassinger, R. Fischer, T. Vence, and J. Huber, "Precoding in multi-antenna and multi-user communications," IEEE Trans. Wirel. Commun., vol.3, no.4, pp.1305-1316, July 2004.
- [12] I. Cosovic, S. Sand, and R. Raulefs, "A non-linear precoding technique for downlink MC-CDMA," IEEE 61st VTC, vol.3, pp.1711-1715, Stockholm, Sweden, May/June 2005.
- [13] T. Itagaki and F. Adachi, "Joint frequency-domain equalization and antenna diversity combining for orthogonal multicode DS-SS-CDMA signal transmissions in a frequency-selective fading channel," IEICE Trans. Commun., vol.E87-B, no.7, pp.1954-1963, July 2004.
- [14] G.H. Golub and C.F. Van Loan, Matrix Computations, 2nd ed., Johns Hopkins University Press, 1989.
- [15] P. Castro and L. Castedo, "Adaptive Tomlinson-Harashima precoding for wireless communication systems," 6th Baiona Workshop on Signal Processing in Communications, Baiona, Spain, Sept. 2003.
- [16] J.G. Proakis, Digital communications, 2nd ed., McGraw-Hill, 1995.
- [17] F. Adachi and K. Takeda, "Bit error rate analysis of DS-SS-CDMA with joint frequency-domain equalization and antenna diversity combining," IEICE Trans. Commun., vol.E87-B, no.10, pp.2991-3002, Oct. 2004.
- [18] H.G. Myung, J. Lim, and D.J. Goodman, "Single carrier FDMA for uplink wireless transmission," IEEE Veh. Tech. Mag., vol.3, no.1, pp.30-38, Sept. 2006.

Appendix A: Noise Power

The noise $\psi(i)$ in Eq. (16) can be rewritten as

$$\psi(i) = \sum_{p=0}^{N_c-1} Q_{i,p}^* \hat{n}(p). \quad (\text{A} \cdot 1)$$

The noise power $\sigma^2(i)$ is obtained from

$$\sigma^2(i) = \frac{1}{2} E[|\psi(i)|^2] = \frac{1}{2} \sum_{p=0}^{N_c-1} \sum_{p'=0}^{N_c-1} Q_{i,p}^* Q_{i,p'} E[\hat{n}(p) \hat{n}^*(p')], \quad (\text{A} \cdot 2)$$

where $\hat{h}(p)$ is given by

$$\hat{h}(p) = \frac{1}{N_c} \sum_{k=0}^{N_c-1} w(k) \Pi(k) \exp\left(j2\pi k \frac{p}{N_c}\right) \quad (\text{A.3})$$

with

$$\Pi(k) = \sum_{t=0}^{N_c-1} n(t) \exp\left(-j2\pi k \frac{t}{N_c}\right) \quad (\text{A.4})$$

being the k th frequency of the noise $n(t)$ due to the additive white Gaussian noise (AWGN) having the one-sided power spectrum density N_0 . Since $E[n(p)n^*(p')] = (2N_0/T_s)\delta(p-p')$, we have

$$\begin{aligned} E[\hat{h}(p)\hat{h}^*(p')] &= \frac{1}{N_c^2} \sum_{k=0}^{N_c-1} \sum_{k'=0}^{N_c-1} w(k)w^*(k') \\ &\quad \times E[\Pi(k)\Pi^*(k')] \exp\left(j2\pi k \frac{kp - k'p'}{N_c}\right) \\ &= \frac{1}{N_c} \frac{2N_0}{T_s} \sum_{k=0}^{N_c-1} |w(k)|^2 \exp\left(j2\pi k \frac{p-p'}{N_c}\right). \end{aligned} \quad (\text{A.5})$$

Hence, we have

$$\begin{aligned} \sigma^2(i) &= \frac{1}{N_c} \frac{N_0}{T_s} \sum_{k=0}^{N_c-1} |w(k)|^2 \\ &\quad \times \sum_{p=0}^{N_c-1} \sum_{p'=0}^{N_c-1} Q_{i,p}^* Q_{i,p'} \exp\left(j2\pi k \frac{p-p'}{N_c}\right) \\ &= \frac{1}{N_c} \frac{N_0}{T_s} \sum_{k=0}^{N_c-1} |w(k)|^2 |Q_i(k)|^2. \end{aligned} \quad (\text{A.6})$$

Appendix B: Discussion of Diagonal Components of \mathbf{R}

Below, we discuss why the diagonal components of \mathbf{R} , corresponding to symbol positions close to the end of signal block, drop. Using joint THP/FDE, the equivalent channel matrix $\hat{\mathbf{h}}$ is transformed into \mathbf{QR} , where \mathbf{R} is the upper triangular matrix and \mathbf{Q} is the unitary matrix. Using the Gram-Schmidt orthogonalization method [14], at first, the norm of the 0th column vector of $\hat{\mathbf{h}}$ is normalized to 1 and this column vector is denoted by \mathbf{q}_0 . Next, after subtracting \mathbf{q}_0 from the 1st column vector of $\hat{\mathbf{h}}$, the norm of the 1st column vector of $\hat{\mathbf{h}}$ is normalized to 1 and its vector is denoted by \mathbf{q}_1 . \mathbf{q}_0 and \mathbf{q}_1 are given by

$$\begin{cases} \mathbf{q}_0 = \frac{1}{R_{0,0}} \hat{\mathbf{h}}_0 \\ \mathbf{q}_1 = \frac{1}{R_{1,1}} (\hat{\mathbf{h}}_1 - R_{0,1} \mathbf{q}_0), \end{cases} \quad (\text{A.7})$$

where

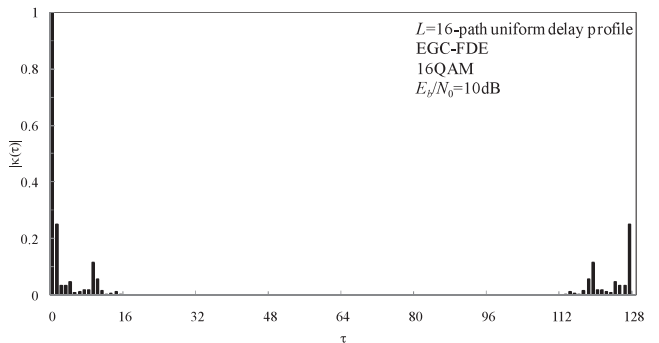
$$\begin{cases} R_{0,0} = \|\hat{\mathbf{h}}_0\|, & R_{0,1} = \frac{\hat{\mathbf{h}}_0^H \hat{\mathbf{h}}_1}{\|\hat{\mathbf{h}}_0\|} \\ R_{1,1} = \|\hat{\mathbf{h}}_1 - R_{0,1} \mathbf{q}_0\| = \left\| \hat{\mathbf{h}}_1 - \frac{1}{\|\hat{\mathbf{h}}_0\|^2} (\hat{\mathbf{h}}_0^H \hat{\mathbf{h}}_1) \hat{\mathbf{h}}_0 \right\|. \end{cases} \quad (\text{A.8})$$

In a similar way, $\{\mathbf{q}_i; i = 0 \sim N_c - 1\}$ and $\{R_{i,j}; i = 0 \sim N_c - 1, j = 0 \sim i\}$ are obtained by repeating the above operations. From Eq. (A.8), it can be understood that $|R_{i,i}|$ is affected by the correlation between the i th column vector and the $0 \sim i - 1$ th column vectors of $\hat{\mathbf{h}}$. As the correlation get stronger, the value of $|R_{i,i}|$ becomes smaller.

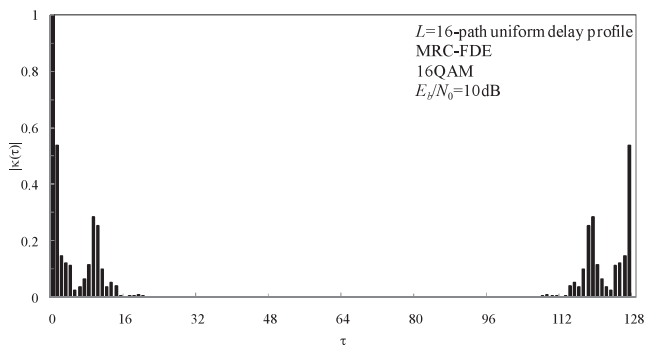
We introduce the normalized correlation between the 0th and τ th column vectors of $\hat{\mathbf{h}}$ given by

$$\kappa(\tau) = \frac{(\hat{\mathbf{h}}_0 \cdot \hat{\mathbf{h}}_\tau)}{(\hat{\mathbf{h}}_0 \cdot \hat{\mathbf{h}}_0)} = \frac{\sum_{l=0}^{N_c-1} \hat{h}_l \hat{h}_{(\tau+l) \bmod N_c}^*}{\sum_{l=0}^{N_c-1} |\hat{h}_l|^2}. \quad (\text{A.9})$$

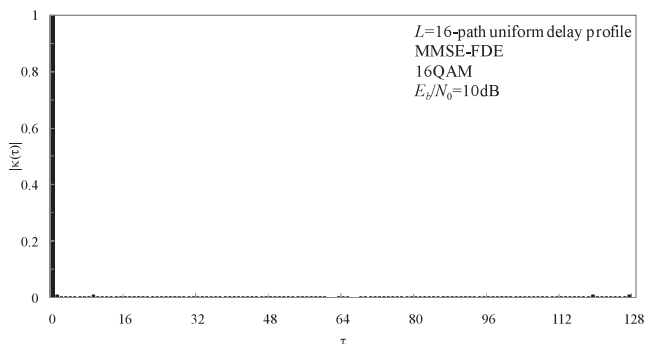
Figure A.1 plots $|\kappa(\tau)|$. Since $\hat{\mathbf{h}}$ is a circulant matrix, $|\kappa(\tau)|$ is a symmetric function about $\tau=64$. As seen from Figs. A.1(a) and (b), the correlation is strongest when $\tau=1$



(a) EGC-FDE



(b) MRC-FDE



(c) MMSE-FDE

Fig. A.1 $|\kappa(\tau)|$.

and 127. Therefore, $|R_{i,i}|$ drops at the symbol position close to $i = N_c - 1$ for EGC and MRC. On the other hand, when MMSE is used, $\kappa(\tau) \approx \delta(0)$ and therefore, column vectors of $\hat{\mathbf{h}}$ are almost orthogonal to each other. Therefore, $|R_{i,i}|$ is almost constant when MMSE is used.



Kazuki Takeda received his B.S. degree in communications engineering from Tohoku University, Sendai, Japan, in 2006. Currently he is a graduate student at the Department of Electrical and Communications Engineering, Tohoku University. His research interests include precoding and channel equalization techniques for mobile communication systems. He was a recipient of the 2007 IEICE RCS (Radio Communication Systems) Active Research Award.



Hiromichi Tomeba received his B.S. and M.S. degrees in communications engineering from Tohoku University, Sendai, Japan, in 2004 and 2006. Currently he is a Japan Society for the Promotion of Science (JSPS) research fellow, studying toward his Ph.D. degree at the Department of Electrical and Communications Engineering, Graduate School of Engineering, Tohoku University. His research interests include frequency-domain equalization and antenna diversity techniques for mobile communication systems. He was a recipient of the 2004 and 2005 IEICE RCS (Radio Communication Systems) Active Research Award.

He was a recipient of the 2004 and 2005 IEICE RCS (Radio Communication Systems) Active Research Award.



Fumiya Adachi received the B.S. and Dr.Eng. degrees in electrical engineering from Tohoku University, Sendai, Japan, in 1973 and 1984, respectively. In April 1973, he joined the Electrical Communications Laboratories of Nippon Telegraph & Telephone Corporation (now NTT) and conducted various types of research related to digital cellular mobile communications. From July 1992 to December 1999, he was with NTT Mobile Communications Network, Inc. (now NTT DoCoMo, Inc.), where he

led a research group on wideband/broadband CDMA wireless access for IMT-2000 and beyond. Since January 2000, he has been with Tohoku University, Sendai, Japan, where he is a Professor of Electrical and Communication Engineering at the Graduate School of Engineering. His research interests are in CDMA wireless access techniques, equalization, transmit/receive antenna diversity, MIMO, adaptive transmission, and channel coding, with particular application to broadband wireless communications systems. From October 1984 to September 1985, he was a United Kingdom SERC Visiting Research Fellow in the Department of Electrical Engineering and Electronics at Liverpool University. He was a co-recipient of the IEICE Transactions best paper of the year award 1996 and again 1998 and, also a recipient of Achievement award 2003. He is an IEEE Fellow and was a co-recipient of the IEEE Vehicular Technology Transactions best paper of the year award 1980 and again 1990 and also a recipient of Avant Garde award 2000. He was a recipient of Thomson Scientific Research Front Award 2004.